Shear Lag Effect and Uncertainty in Concrete Box Girder Creep

By Vladimír Křístek[1] and Zdeněk P. Bažant,[2] F. ASCE

Abstract: The effect of shear lag on creep deformations and stress redistributions in concrete box girder bridges is analyzed both deterministically and stochastically. It is found that the shear lag is as important for creep as it is for elastic deformations. Compared to bending theory predictions, the shear lag causes a significant increase in the maximum longitudinal normal stress, alters the stress redistributions due to a change in the structural system during the construction stage, and substantially increases the deflections. The statistical variability of material creep parameters and environmental factors has a significant effect on the statistical scatter of the calculated maximum longitudinal stresses and a very large effect on the statistical scatter of the predicted deflections. Both the shear lag effect and the statistical variability of creep must be taken into account if a reliable design of box girder bridges from the viewpoint of long-term serviceability should be achieved.

Introduction

Since shear lag has been shown (13,15–18,22) to substantially affect the deformations and stresses in prestressed concrete box girder bridges, the same must be expected for creep. The purpose of this study is to analyze this problem and assess the magnitude of the effect. The shear lag will be considered concurrently with other previously analyzed salient aspects of creep in prestressed concrete bridges, which include the influence of aging, the stress redistributions caused by changes in the structural system during the construction stages, and the random nature of response caused by uncertainties in the values of material parameters as well as environmental factors (2,3,7,8,11,21).

In a box girder [Fig. 1(*a*)], a large shear flow is normally transmitted from the vertical webs to the horizontal flanges. This causes in-plane shear deformations of the flange plates, the consequence of which is that the longitudinal displacements in the central portion of the flange plate lag behind those near the web, whereas the bending theory predicts equal displacements. Thus, the shear lag produces out-of-plane warping of an initially planar cross section [Fig. 1(*b*)] and a significant nonuniformity of the distribution of the longitudinal normal stress σ across the flange width, as shown in Fig. 1(*a*). Calculations according to the bending theory, which assumes the plane cross sections to remain plane and thus neglects the shear lag, underestimate the stresses in the flange plates at locations adjacent to the webs. This reduces the margin of safety against

[1]Visiting Scholar, Ctr. for Concrete and Geomaterials, Northwestern Univ.; Research Prof. on leave from the Faculty of Civ. Engrg., Czech Technical Univ. at Prague, (ČVUT), Thákurova 7, 16629 Praha 6, Czechoslovakia.

[2]Prof. of Civ. Engrg. and Dir., Ctr. for Concrete and Geomaterials, Northwestern Univ., Tech 2410, Evanston, IL 60201.

Note.—Discussion open until August 1, 1987. To extend the closing date one month, a written request must be filed with the ASCE Manager of Journals. The manuscript for this paper was submitted for review and possible publication on February 20, 1986. This paper is part of the *Journal of Structural Engineering*, Vol. 113, No. 3, March, 1987. ©ASCE, ISSN 0733-9445/87/0003-0557/$01.00. Paper No. 21331.

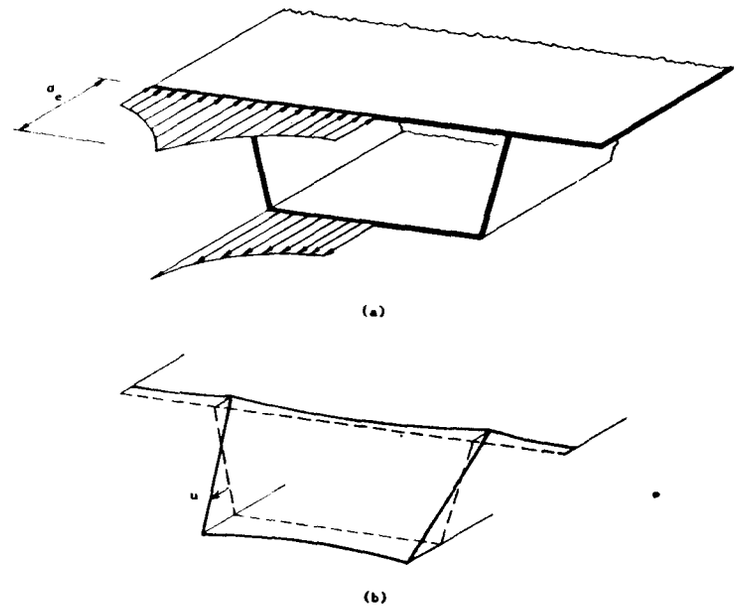

FIG. 1.—(*a*) Typical Box Cross Section and Nonuniformity of Longitudinal Stress Distribution Caused by Shear Lag; and (*b*) Out-of-Plane Warping

cracking. Even more important is the increase of box girder deflections caused by the shear lag.

The shear lag effect increases with the width of the box, and so it is particularly important for modern bridge designs which often feature wide single-cell box cross sections. The shear lag effect becomes more pronounced with an increase in the ratio of the box width to the span length, which typically occurs in the side spans of bridge girders. The nonuniformity of the longitudinal stress distribution is particularly pronounced in the vicinity of large concentrated loads, such as the pier reactions or the reactions from cables in cable-stayed bridges. Aside from its adverse influence on the transverse stress distribution and the deflection of the bridge, the shear lag also alters the longitudinal bending moment and shear force distributions in redundant structural systems. Finally, the effect of the shear lag on the shear stress distribution in the flange of the box, as compared to the prediction of bending theory, is also appreciable.

A typical situation in which large stress redistributions are caused by creep is the development of a negative bending moment over the support when two adjacent spans are initially erected as separate simply supported beams and are subsequently made continuous over the support. In absence of creep, the bending moment over the support due to own weight remains zero, and thus the negative bending moment which develops is entirely caused by creep. This study, on which a brief preliminary report was made at a recent conference (6), will investigate what the roles of creep and material uncertainty are in this phenomenon.

METHOD OF ANALYSIS

In the present study, consideration is restricted to a linear creep law, which implies applicability of the principle of superposition. The linearity assumption is admissible since our attention will be restricted to stresses in the service stress range, which may not exceed 0.4 of the standard cylindrical compression strength according to AASHTO specifications. Although the linearity assumption might not be very accurate even in the service stress range when the concrete structure undergoes humidity and temperature changes, a nonlinear creep law for drying concrete, while more realistic, would be too complicated for the scope of the present study. To be able to neglect the effect of cracking, we must also assume that there is sufficient prestress to prevent it.

The linear creep and elastic properties are fully characterized by the compliance function $J(t,t')$ which defines the strain at age t caused by a unit constant uniaxial stress applied at age t'. Because creep depends not only on the load duration $t - t'$ but also on the age at loading t', the aging effect is implied in the compliance function. The reduction of the average creep coefficient caused by prestressed and mild reinforcement is neglected in our calculation, as is customary in design practice.

A realistic prediction of the compliance function of concrete from the mix characteristics, design strength, and the curing and environmental conditions is made possible by the BP model (9). In this model, the basic creep curves are described in terms of the double power law. Recently, it has been found that creep properties for very long load durations which are of particular interest in bridge design are better described by a refinement of the double power law, called the triple power law (5). Since the accuracy of the material characterization should be commensurate with the accuracy of structural analysis, it seems appropriate to use the more accurate triple power law when refinements such as the shear lag are introduced in creep structural analysis. In all our calculations, the triple power law will be used instead of the double power law in conjunction with the drying creep term of the BP model as originally defined by Bažant and Panula (9,10).

For the purpose of assessing the effect of construction stages, the creep analysis of an arbitrary continuous girder with its various possible support conditions can be performed, as an approximation, in two successive stages, as shown in Fig. 2. In this approach, the distributions of bending moment and shear force are first determined by an ordinary creep analysis (8,11,21) which respects the changes of the structural system during construction but neglects the shear lag [Fig. 2(*a*,*b*)]. This analysis yields the locations of the inflection points at which the bending moment is zero. The portion of the girder between these inflection points may be treated as a simply supported beam or a cantilever. Based on the shear force distribution, the system of loads or reactions acting on each portion of the girder can be evaluated [Fig. 2(*c*)], and the shear lag analysis can then be carried out independently for each individual portion of the girder.

The error of this approach, probably not too serious, is that the shear lag causes additional flexibility of the girder and in this manner also influences the distribution of the bending moment and thus the loca-

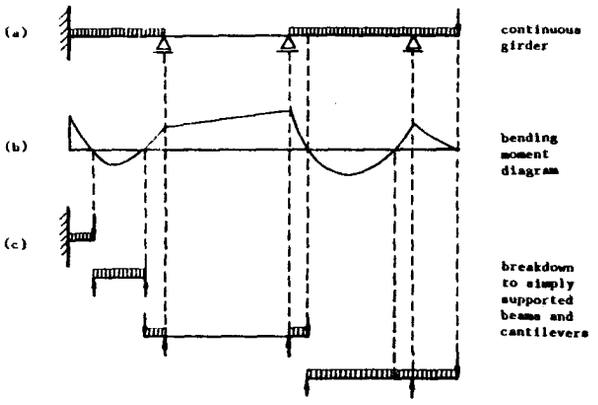

FIG. 2.—Approximate Analysis of Continuous Girder by a Reduction to Statically Determinate Segments

tions of the cross sections with a zero bending moment. Furthermore, these locations shift in time.

In each statically determinate portion of the beam obtained in this manner [Fig. 2(*c*)], the shear lag effects can in general be computed by many of the existing commercial finite element shell programs as well as by programs based on the more classical folded plate theory. Computationally, however, it is most efficient to apply the Fourier series solution which was previously developed specifically for the shear lag analysis in box girders (17,18) and was shown to converge very rapidly. The Fourier series solution according to the folded plate theory accounts for both elastic plate bending and general in-plane deformations of the plates for which the longitudinal normal strains and stresses are not required to be distributed linearly.

Although this solution method is most directly applicable to the case of a simply supported box girder, a cantilever box girder may also be analyzed (16) by means of a substitute simply supported beam as shown in Fig. 3. In this approach, a mirror image of the cantilever about its

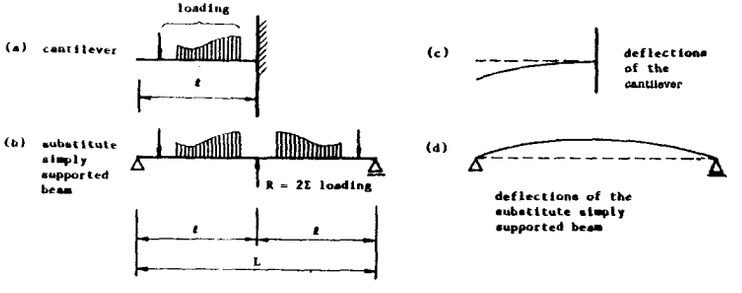

FIG. 3.—Replacement of Cantilever Analysis by Analysis of a Substitute Simply Supported Beam

clamped end is created and a force R (Fig. 3) is applied at the midspan of the substitute girder thus obtained, in order to balance the applied load [Fig. 3(*b*)]. This brings the substitute girder consisting of the cantilever and its mirror image into a state of equilibrium, and dummy simple supports may be imagined at the ends of this girder [Fig. 3(*b*)]. No reactions arise at these dummy supports, of course, and the stresses developed in the substitute and the actual girders are identical.

As a more accurate approach which avoids the error due to the shear lag effect on the location of the cross section with a zero bending moment, the initial stress procedure can be applied. The construction and life span of the girder is divided into time intervals, the duration of which can be as long as the duration of each construction stage provided the girder is homogeneous. First, the stress relaxation in the girder is calculated and the forces violating equilibrium are evaluated. Subsequently these forces are applied to the girder acting in a new structural system in the next construction stage, and their effect is then analyzed, e.g., by the finite element method or the folded plate theory (13,15,22); see Appendix I.

In the present calculations, the age-adjusted effective modulus method (2), endorsed by an ACI Committee 209 Recommendation (1), is employed. According to this method, the relaxation of stress in a restrained structure is characterized by the relaxation ratio (2):

$$r(t) = \frac{\sigma(t)}{\sigma(t_r)} = 1 - \frac{\phi(t,t_0) - \phi(t_r,t_0)}{1 + \chi(t,t_r)\,\phi(t,t_r)}; \quad (t \geq t_r) \ldots\ldots\ldots\ldots\ldots\ldots\ldots\ldots (1)$$

in which $\phi(t,t_0)$ = the creep coefficient determined on the basis of the compliance function (11); $\chi(t,t_r)$ = the aging coefficient, t_0 = the age of concrete when the girder begins carrying its own weight; t_r = the age at which the simply supported girder spans are made continuous, i.e., at which the relaxation process starts and the girder becomes redundant; and t = the final time under consideration.

The calculation procedure just outlined yields a deterministic solution. However, along with shrinkage, creep is the most uncertain mechanical property of concrete. Therefore, the stochastic nature of creep ought to be taken into account in the design of box girder bridges. This can be most simply accomplished by a sampling approach which reduces a probabilistic analysis to a series of deterministic structural analyses. The most effective approach known is the Latin hypercube sampling (7), which greatly reduces the computational work compared to other sampling techniques and has already been applied to the probabilistic analysis of creep and shrinkage effects in beam structures (7). The procedure of calculation is the same as described on pages 1114–1115 of Ref. 7, and need not be repeated here. It suffices to say that the Latin hypercube sampling is a method to randomly generate, according to the specified probability distributions of the random parameters affecting creep, a finite set of parameter samples of equal probability. For each such set, a deterministic structural creep analysis, in our case with consideration of the shear lag, is carried out. From the responses obtained for all these samples one can then estimate not only the mean but also the standard deviation s of any response quantity. If the number of samples is very large, the type of distribution can be also estimated. We assume, however, all distributions to be normal, which was shown to be a relatively good assumption in previous studies of creep effects in structures (7).

In particular, the random parameters affecting creep are considered to be the same as in the previous study (7). They consist of environmental relative humidity h, the cement content c per m^3 of concrete, the water-cement ratio w/c (by weight), the sand-cement ratio s/c, the gravel-cement ratio g/c, uncertainty factor Ψ_2 multiplying the magnitude of the basic creep with elastic deformation (Eq. 3 of Ref. 7), uncertainty factor Ψ_3 for the additional creep due to drying (Eq. 3 of Ref. 7), and the design value of the standard cylinder strength of concrete, f'_c. The influence of these parameters is determined according to an improved BP model, in which the triple power law is used instead of the double power law for the basic creep component while the drying creep component is taken from the original BP model (9,10).

Numerical Examples

The effect of shear lag upon creep deflections and stress redistributions in concrete box girder bridges will now be demonstrated by two typical practical examples. Only fully prestressed girders, in which no significant cracking in the cross section planes takes place, are considered.

Lest the shear-lag effect be obviated by other phenomena which are disregarded in the current design practice, the effects of humidity and temperature variations and of the self-equilibrated nonuniform stress distribution across the plate thickness which they produce will be left out of consideration, even though they may cause extensive cracking or strain softening and make the average creep properties of the cross section dependent on the size and configuration of the cross section. Due to the strong nonuniformity of the stress distribution across the plates of the cross section, which is caused by humidity and temperature effects, only the stress average over the plate thickness is practically meaningful if the foregoing effects are disregarded in the analysis. Therefore, the stresses will be evaluated at the middle of the plate thicknesses rather than at the top and bottom faces of the plates which form the box. The primary intent of our analysis will be to demonstrate the effect of the shear lag on the deflections as well as the creep stress redistributions due to a change in the structural system during the construction stage.

As the first example, we consider a pair of two simply supported beams which are made continuous over the support after they have already started carrying their own weight. A cross section of a simplified shape shown in Fig. 4(*a*) is considered. The dimensions indicated are for the midplanes of top and bottom plates and webs of the box. The elevation of the bridge is shown in Fig. 4(*b*). The analysis is made under the assumption that there is a deformable diaphragm 400 mm thick above the inner support, but not within the spans. The diaphragms above the end supports are assumed to be infinitely rigid in their own plane. The girder spans are assumed to start carrying their dead load at the age of t_0 = 28 days. At the age t_r = 35 days the box girder spans are joined above the inner support to form the final structural system—a continuous girder.

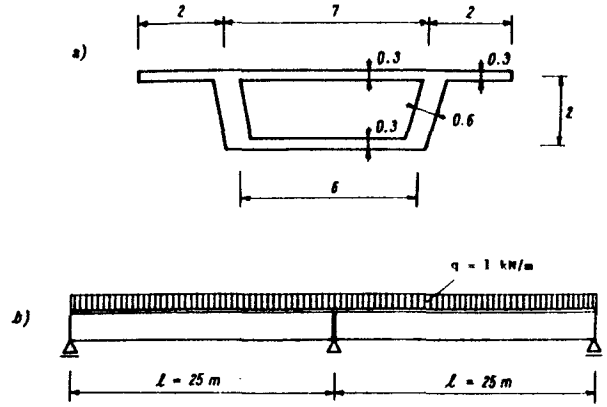

FIG. 4.—(*a*) Box Cross Section Considered in Examples; (*b*) Girder Analyzed in the First Example

Only the dead load, taken as unity, i.e., $g = 1$ kN/m, is considered in our analysis. The other loads, including the secondary moments due to prestressing, can be analyzed separately and the results superimposed since the principle of superposition is valid.

First we carry out a deterministic analysis, using the mean values of all parameters as specified in Col. 10 of Table 1. The typical values of the compliance function $J(t,t')$ obtained from the triple power law and the BP model are also listed, and so are the conventional static modulus E_{28} at the age of 28 days, and the values of the creep coefficient $\phi(t,t')$. The deterministic analysis is first carried out in the usual manner, i.e., according to the bending theory, in which the shear lag effect is neglected. The bending moment distribution obtained for the time $t = 10{,}000$ days is plotted in Fig. 5(*a*) as the dashed curves. Note that the bending moment above the inner support, which was initially zero, attains a large magnitude due to creep. The calculation (based on the data in the last column of Table 1) yields for the longitudinal stresses above the inner support the following maximum values: (1) At the mid-plane of the top flange: $\sigma_t = 0.802 \times 52.81/5.665 = 7.477$ kN/m^2; (2) at the mid-plane of the bottom flange: $\sigma_b = -1.198 \times 52.81/5.665 = -11.17$ kN/m^2. The transverse distributions of the longitudinal stresses at the mid-thickness of the walls are plotted as the dashed lines in Fig. 5(*c*).

As mentioned before and justified in detail in Appendix I, the exact linear solution which considers the shear lag is carried out in two successive stages. In the first stage, the pair of the two simply supported beams is imagined to be held at constant deformation, and the stresses then relax from time t_r to time t in proportion to function $r(t)$. In the second stage, a fictitious distributed load of magnitude $1 - r = 0.676$ kN/m is applied on the continuous two-span box girder in its final form. Due to linearity, McHenry's elastic-viscoelastic analogy (4) applies. Since the structure is considered to be homogeneous in its creep properties, the stresses may be simply obtained according to the elasticity theory, by applying the usual folded plate analysis in terms of trigonometric

TABLE 1.—Eight Sets of Random Parameter Samples, with Corresponding Values of Compliance Function, Elastic Modulus and Creep Coefficient ϕ

Random parameter (1)	Run Number 1 (2)	2 (3)	3 (4)	4 (5)	5 (6)	6 (7)	7 (8)	8 (9)	Mean values (10)	Standard deviation (11)
h	0.713	0.849	0.765	0.586	0.670	0.451	0.535	0.630	0.650	0.13
c	381.05	344.49	318.95	403.69	355.51	296.30	332.89	367.11	350	35
w/c	0.508	0.692	0.653	0.591	0.629	0.571	0.547	0.609	0.6	0.06
s/c	2.177	1.969	1.693	1.902	2.098	2.306	1.823	2.031	2	0.2
g/c	3.266	3.147	2.853	2.743	3.047	3.460	2.953	2.540	3	0.3
Ψ_2	1.353	0.964	1.112	0.796	0.888	0.647	1.203	1.036	1	0.23
Ψ_3	0.936	0.980	1.200	0.885	1.064	0.800	1.115	1.020	1	0.13
f'_c (MPa)	39.81	35.02	31.39	32.78	36.17	29.14	33.93	37.56	34.48	3.475
$J(35, 28)10^{-5}$ MPa^{-1}	5.548	4.574	7.001	3.920	4.618	4.089	6.897	5.061	5.137	—
$J(10{,}000, 28)10^{-5}$ MPa^{-1}	11.08	9.802	16.24	9.365	11.71	10.79	16.96	11.24	12.258	—
$J(10{,}000, 35)10^{-5}$ MPa^{-1}	10.71	9.457	15.66	9.045	11.31	10.42	16.38	10.86	11.839	—
E_{28} MPa	41,287	37,467	29,586	38,588	38,573	32,236	33,673	37,249	36,944	—
$\phi(35, 28)$*	1.29	0.71	1.07	0.51	0.78	0.318	1.32	0.88	0.90	—
$\phi(10{,}000, 28)$*	3.57	2.67	3.81	2.61	3.51	2.48	4.71	3.19	3.53	—
$\phi(10{,}000, 35)$*	3.42	2.54	3.63	2.49	3.36	2.36	4.52	3.05	3.37	—

*Here $\phi(t,t') = E_{28}\,J(t,t') - 1$, not $E(t')\,J(t,t') - 1$.

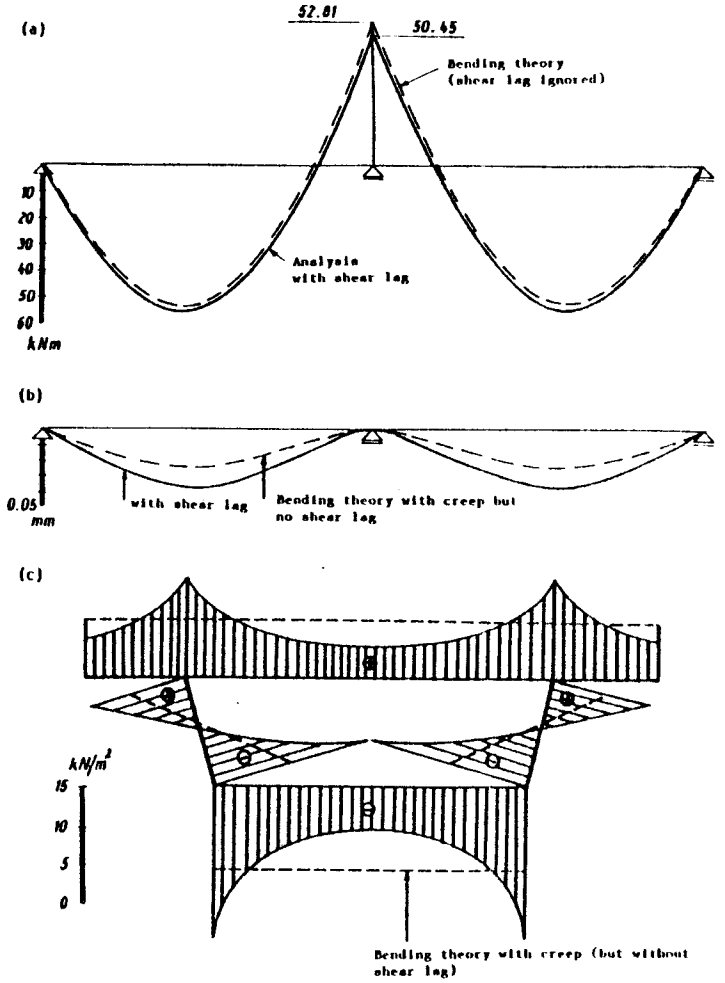

FIG. 5.—Results of First Example [Fig. 4(*a*, *b*)]: (*a*) Bending Moment Distributions at 10,000 Days; (*b*) Increase of Deflections from 35 Days to 10,000 Days; and (*c*) Transverse Distributions of Longitudinal Stresses at 10,000 Days

series (13,15,22). The resulting stress state of the box girder at $t = 10{,}000$ days is obtained as the sum of the stresses obtained in both stages.

The resulting distribution of the longitudinal stresses throughout the cross section above the inner support is plotted in Fig. 5(*c*) as the solid curves. Note that this solution yields in the vicinity of the webs much higher stresses than does the bending theory which neglects the shear lag [the dashed lines in Fig. 5(*c*)]. Also note the pronounced nonlinearity of the longitudinal stress distribution along the depth of the web. This nonlinearity of the stress distributions and the occurrence of the sharp peaks near the bottom flange edges are due to the concentrated nature of the reaction from the support. While the webs transmit a larger portion of the bending moment above the support, the longitudinal forces

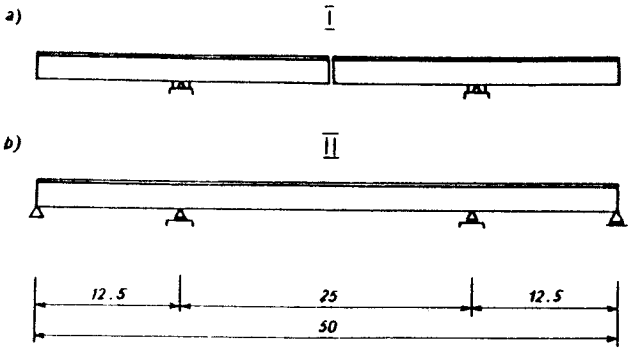

FIG. 6.—Second Example: (*a*) Initial Structural System during Construction; (*b*) Final Structural System

and bending moments transmitted by the top and bottom plates are somewhat relieved due to the effect of the shear lag.

The shear lag significantly increases the flexibility of the girder, especially in the inner support region. As a consequence of this, the bending moment distribution is altered to that shown in Fig. 5(*a*) by the solid curves. The bending moment above the inner support is found to be reduced due to the shear-lag effect by about 5%, as compared with the result of bending theory. On the other hand, the bending moment that arises at the midspan is increased.

Modest though the changes of the bending moments are, the effect of the shear lag is large as far as the deflections are concerned. This is seen from the results plotted in Fig. 5(*b*) in which the dashed and solid curves show the calculated long-time deflections at the time of 10,000 days when the shear lag is neglected or is taken into account, respectively. The ordinate plotted in this diagram is the deflection increment after the girder is made continuous, i.e., the deflection caused by the creep after time t_1. These results show that the usual calculation based on the bending theory which neglects the shear lag underestimates the long-time creep deflections by about 33% of the correct midspan deflection, i.e., the true deflection is about 50% larger than the bending theory prediction. Thus, the shear lag effect might help to explain why the long-time deflections observed in practice often greatly exceed the design values.

As the second example, we consider a three-span girder created by joining in the middle of the central span a pair of segmentally cast cantilevers [Fig. 6(*a*)] and by inserting additional supports at the girder ends [Fig. 6(*b*)]. The time at mid-span joining and adding of the end supports is $t_1 = 35$ days. The same simplified cross-section as before is considered [Fig. 4(*a*)] and a unit uniform distributed load is assumed.

Fig. 7(*a*) shows the deflection curve, and Fig. 7(*b*) the bending moment distribution. The transverse distributions of the longitudinal stresses at the midthickness of walls are seen in Fig. 7(*c*), plotted for the central cross section of the middle span. In this particular cross-section all the bending moment is caused by creep, since without creep it would re-

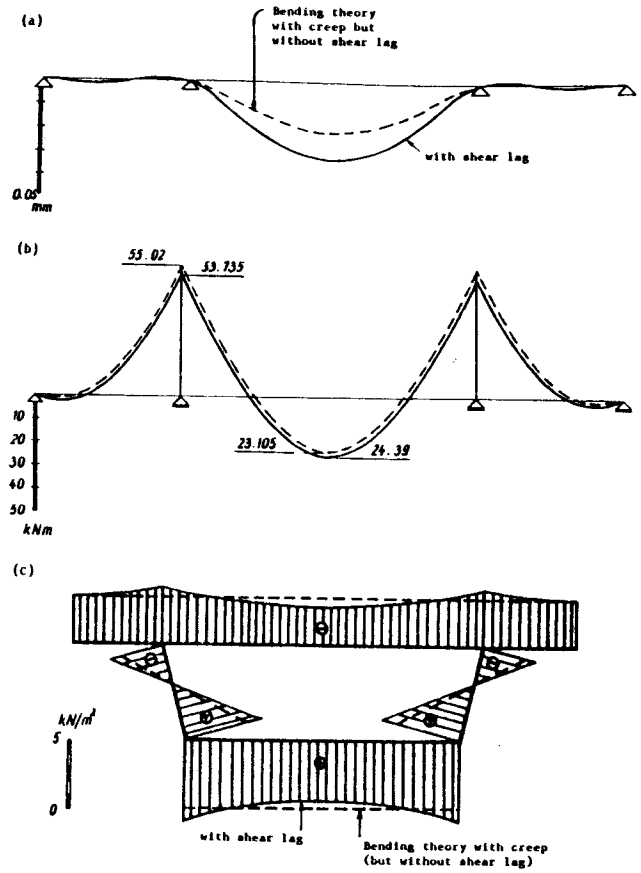

FIG. 7.—(*a*) Deflection Increase from 35 to 10,000 Days; (*b*) Bending Moment Distributions at 10,000 Days; (*c*) Transverse Distributions of Longitudinal Stress in the Middle of Central Span at 10,000 Days

main zero, same as before the joining of cantilevers. However, the nonuniformity of the transverse stress distributions in this cross section happens to be the minimum for the entire girder. The shear lag effect per se is maximum in the cross sections above the inner supports, at which large concentrated reactions are applied, and is large in the side spans as well.

In all the diagrams, the results obtained with the consideration of shear lag (solid lines) are compared with the results of the bending theory, which are shown by the dashed lines. The comparisons again demonstrate the importance of shear lag. In this second example, the additional deflection due to the shear lag [Fig. 7(*a*)] is even larger than in our first example [Fig. 5(*b*)]. This is probably explained by the fact that the deflections at the midspan are reduced by the support bending moments acting at both ends, as well as the fact that the width-to-length ratio of the box girder in the side spans is larger than in the first example, making the stiffness reduction due to the concentrated nature of the support reaction relatively more pronounced.

Response Statistics

Due to the notorious statistical variability of creep predictions, structures should be designed for certain extreme effects exceeded with a specified small probability, such as 5%, rather than for the mean effects as is customary at present. This approach seems particularly important for box girder bridges since excessive deflections and damages due to cracking have been experienced on this type of bridges built in the past.

The solution depends on eight random parameters whose means and standard deviations, taken from a previous work (7,19), are listed in the last two columns of Table 1. We assume all these parameters to be independent (which is certainly a simplification) and their distributions to be normal. A certain number of different random parameter samples, chosen as 8 and 16, and given for the case of 8 in Table 1, may then be generated according to the method of Latin hypercube sampling (7). These random samples are all of equal probabilities. For the set of material parameter values for each sample, i.e., for each of the columns of Table 1, the solution is calculated deterministically as already described. The results for the individual random samples of material parameters, as obtained for the stress in the top corner of the box and for the midspan deflection (for the first example of the two-span girder made continuous, Figs. 4 and 5) are arranged according to their magnitudes, and their cumulative frequency distribution may be plotted as shown in Fig. 8(*a–b*) for 8 samples and in Fig. 8(*c–d*) for 16 samples. If the plot is made on the normal probability scale, the slope of the regression line is an estimate of the standard deviation s, and the ordinate at 50% is the mean, $\bar{y}$ [Fig. 8(*a–b*)]. The standard deviation may also be obtained as $s = y(0.842) - \bar{y}$ where $y(0.842)$ is the value of the ordinate of the regression line at 84.2%.

There are various ways to construct the cumulative frequency distribution plots shown in Fig. 8. As proposed by Blom (12) and proven by Kimball (14,20), the optimum type of plot is given by the points $[(i - 0.375)/(n + 0.25), y_i]$ where n is the number of all points and y_i ($i = 1, 2, 3, \ldots n$) is an ordered set of the values plotted, ordered so that $y_1 \leq y_2 \leq \ldots \leq y_n$. This type of plot is superior to the plots $[(i - 0.5)/n, y_i]$ or $[i/(n + 1), y_i]$, which are customarily used. The mean and standard deviation may be estimated from the set of all results y_i without constructing the cumulative frequency plot, simply from the formulas $\bar{y} = \Sigma\, y_i/n$, $s = [\Sigma\, (y_i - \bar{y})^2/n]^{1/2}$. The value of the graphical plot is that it indicates how consistent the results are and whether they are normally distributed. If their distribution were perfectly normal, the points in Fig. 8 would have to lie on a straight line, and so the deviations from the straight regression line indicate deviations from the normal distribution. In our case, the points do deviate from the straight regression line [Fig. 8(*a–d*)], however, the deviations are not very large, especially for the case of 16 random samples. Better statistical results could be obtained with a greater number of Latin hypercube samples. The degree of error

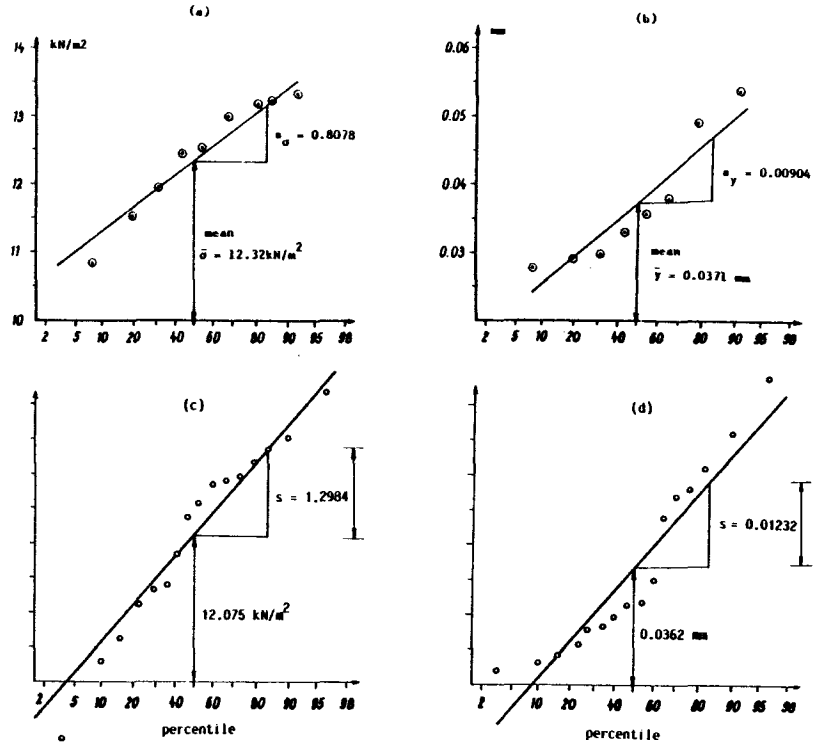

FIG. 8.—Cumulative Frequency Distribution of Sampling Results for: (*a, c*) Longitudinal Stress in Upper Box Corner (8 Samples); and (*b, d*) for Mid-Span Deflection (16 Samples)

in the statistics obtained may also be assessed by repeating the entire calculation with the same number of samples randomly generated again. Such studies have been made in Ref. 7, from which it appeared that 16 parameter samples in similar types of problems yield results which are acceptable in view of the many uncertainties involved in the assumptions of the analysis. Although our sets of 8 and 16 random samples yield about the same means $\bar{y}$, as is apparent from Fig. 8, the difference in standard deviations (i.e., slopes in Fig. 8) is quite appreciable. Therefore, the stress and deflection distributions (Fig. 9) are plotted from a set of 16 samples (while the corresponding plots for 8 samples were given in Ref. 6).

Figs. 9(*a–b*) show the statistical results for the transverse distribution of longitudinal stress above the support and the deflection curve for the first example. The values of the mean $\pm 2s$ (s = standard deviation) are plotted. These values represent the 95% confidence limits for the results, i.e., the limits that are exceeded with 2.5% probability on the plus side and 2.5% on the minus side. To assure good long-term serviceability it seems reasonable to require that the design of box girder bridges should be based on these limits.

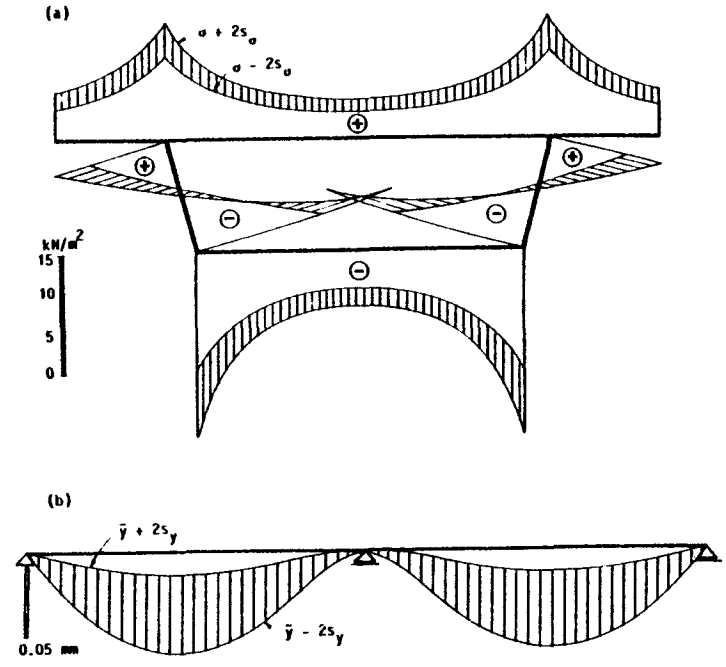

FIG. 9.—Statistical Results for First Example: (*a*) 95% Confidence Limits for Longitudinal Stresses at Support Cross Section; and (*b*) for Deflections at Midspan

We see that the spread of the results for the deflections [Fig. 9(*b*)] is very large, and is, in fact, much larger than that for the stresses [Fig. 9(*a*)]. Nevertheless, even for the stresses, the statistical spread is quite significant for design. The reason that the large statistical scatter of the compliance function values translates into a relatively smaller scatter of the stress values consists in the fact that the redundant (i.e., the moment over the support) is proportional to the quantity:

$$1 - r = \frac{\phi(t, t_0) - \phi(t_r, t_0)}{1 + \chi(t, t_r)\,\phi(t, t_r)} \qquad (2)$$

The greater the creep, the larger is this quantity, but it can never exceed 1 because the relaxation ratio r cannot become negative (for $r = 0$, the redundant value would reach the limiting case of an elastic solution for a monolitically cast girder). Thus, when creep is large, the expression from Eq. 2 is close to 1, and since it cannot exceed one, its statistical scatter must be small no matter how large the scatter of material parameters is.

By contrast, the statistical spread of the creep deflection increments [Fig. 9(*b*)] is larger because, as one can prove (see Appendix I, Eq. 5*b*), it is equal to the deflection w_{el} of an elastic continuous two-span girder (i.e., the girder with its final structural system) caused by applied load (in our case the unit own weight 1 kN/m) multiplied by the increase in the creep coefficient value, i.e.,

$$\Delta w(t, t_r) = \Delta w(10{,}000, 35) = w_{el}\,[J(10{,}000, 28) - J(35, 28)]E \quad \ldots\ldots\ldots \quad (3)$$

in which w is the deflection and E is the elastic modulus used to calculate w_{el}. Thus, the statistical scatter of J is manifested in the statistical scatter of the deflection almost proportionally.

In view of the dismal experience with deflections of some prestressed concrete box girder bridges built in the past, the foregoing observations about the statistical scatter should be taken into account by bridge designers. When the statistical variability just demonstrated is superimposed on the effect of the shear lag on deflections, one can understand that the real deflections of the bridge can be far larger than those obtained by deterministic calculations according to the bending theory, which are customary at present and are permitted by the design codes now in effect. (We have not yet considered the effect of nonuniform humidity and temperature distributions in the structure, which tend to further augment the deflections!)

Finally, it should be emphasized that the statistical spread of the results depends on the accuracy of the creep prediction model. The improved BP model used in this study is relatively complicated but has a much smaller statistical uncertainty than the existing recommendations of ACI or CEB-FIB. These recommendations are considerably simpler, but the standard deviations of the compliance function obtained according to these recommendations are almost twice as large as those of the BP model (10). Thus, the spread of the statistical results for the deflections in Fig. 9(*b*) would approximately *double* if the calculations were carried out according to the existing recommendations of ACI or CEB-FIB.

Conclusions

Shear lag in box girder bridges is as important for long-time creep as it is for short-time elastic behavior. Compared to bending theory predictions, the shear lag effect can significantly increase the maximum values of the stress changes caused by a change of the structural system during construction, and cause a large increase in the long-time deflections. These effects are important especially when the span-to-box-width ratio is small.

The statistical variability of material creep parameters and environmental factors is as important as the shear lag effect. It causes a significant statistical scatter in the predicted long-time stress values, and a large scatter in the predicted long time-deflections.

To achieve a reliable design from the viewpoint of long-time serviceability both the shear lag effect and the statistical scatter must be taken into account in design.

Acknowledgments

Partial financial support under United States National Science Foundation Grant No. CEE-800-3148 to Northwestern University is gratefully acknowledged. Thanks are due to Jan L. Vítek for developing and making available a computer program for rapid evaluation of compliance values according to the triple power law.

Appendix I.—Effects of a Change of Structural System

The constant dead load is applied suddenly at age t_0 on the structure in its initial structural system I, which may be statically determinate or indeterminate. Due to the linearity of the creep law and the assumption that the structure is homogeneous, the stresses remain constant and equal to the initial elastic stresses $\sigma_{el}(\underline{x})$ where $\underline{x} = (x, y, z)$; x is the axial coordinate of the girder and y, z are the transverse cartesian coordinates. At time t_r the structural system is changed to system II by adding to system I further constraints without any sudden change of stresses at time t_r. According to Ref. 4, the easiest method to calculate the effect of this change is as follows: First we imagine the deformations to be frozen from time t_r on, e.g., $\Delta\epsilon(\underline{x}, t) = \epsilon(\underline{x}, t) - \epsilon(\underline{x}, t_r) = 0$. This would cause stress variation $\sigma(\underline{x}, t)$ which satisfies at every location $\underline{x}$ the following equations:

1. For an exact linear solution:

$$\epsilon(\underline{x}, t) - \epsilon(\underline{x}, t_r) = \int_{t_r}^{t} J(t, t')\,\sigma(\underline{x}, dt') + \sigma_{el}(\underline{x})[J(t, t_0) - J(t_r, t_0)] = 0 \quad \ldots\ldots \quad (4a)$$

2. For a simplified solution (by age-adjusted effective modulus method):

$$\epsilon(\underline{x}, t) - \epsilon(\underline{x}, t_r) = \frac{\sigma(\underline{x}, t) - \sigma(\underline{x}, t_r)}{E''(t, t_r)} + \sigma_{el}(\underline{x})[J(t, t_0) - J(t_r, t_0)] = 0 \ldots\ldots \quad (4b)$$

where $\sigma(\underline{x}, dt') = [\partial\sigma(\underline{x}, t')/\partial t']dt'$; and $E''(t, t_r) = E(t_r)/[1 + \chi(t, t_r)\,\phi(t, t_r)]$ = age-adjusted effective modulus. Substituting $\sigma(\underline{x}, t) = r(t)\,\sigma_{el}(\underline{x})$ where $r(t)$ = relaxation ratio, we get from Eq. 4*a* for the exact solution a Volterra integral equation for function $r(t)$, which may be easily solved numerically with high accuracy in a step-by-step manner. For the simplified solution we get from Eq. 4*b* an algebraic linear equation whose solution is the expression for $r(t)$ already given in Eq. 1. Note that $r(t_r) = 1$ and subsequently $r(t)$ monotonically decreases. When $t_r = t_0$, $r(t) = R(t, t_0)/E(t_0)$ where $R(t, t_0)$ is the relaxation function, which can be easiest obtained from an approximate explicit formula (see Eq. 7.20 of Ref. 11). When, however, $t_r > t_0$, $r(t)$ is not proportional to the relaxation function. The greater the difference $t_r - t_0$, the larger is the error of the approximate formula in Eq. 1.

Second, we note that in order to equilibrate the aforementioned stress changes, the applied load (in our case a unit distributed load), must be reduced also by the ratio $r(t)$ (this follows from McHenry's analogy, see Ref. 4). This means that we need to apply on system I an additional uniform load $-[1 - r(t)]$, or remove load $[1 - r(t)]$ from system I.

Third, the deformations are imagined to be unfrozen and the additional load $-[1 - r(t)]$ is canceled by applying, now on system II, the opposite uniform load $[1 - r(t)]$. Only this last load produces deflection changes and stress redistributions after t_r.

Thus, the deflection changes after time t_r and part of the stress changes that are caused after time t_r by the change of the structural system are

obtained as the deflections and stresses caused by the load $[1 - r(t)]$ in the homogeneous structure of structural system II. This part of the stress changes is equal to the elastic stresses produced by the load $[1 - r(t)]$ on strucutral system II. The corresponding deflection changes $w^{II}(\underline{x}, t)$ are calculated as:

1. For an exact linear solution:

$$w^{II}(\underline{x}, t) = w^{II}_{el}(\underline{x})\, E(t_r) \int_{t_r^+}^{t} J(t, t') \frac{d}{dt'} [1 - r(t')] dt' \quad \ldots\ldots (5)$$

$$\text{or} \quad w^{II}(\underline{x}, t) = -w^{II}_{el}(\underline{x})\, E(t_r) \int_{t_r^+}^{t} J(t, t')\, dr(t') \quad \ldots\ldots (6)$$

2. For a simplified solution, with $r(t)$ substituted according to Eq. 1, and $\phi(t, t_r) = E(t_r)\, J(t, t_r) - 1$:

$$w^{II}(\underline{x}, t) = w^{II}_{el}(\underline{x}) \frac{E(t_r)}{E''(t, t_r)} [1 - r(t)] \quad \ldots\ldots (7)$$

After substituting $E'' = E/(1 + \chi\phi)$ and Eq. 1 for $r(t)$, we get:

$$w^{II}(\underline{x}, t) = w^{II}_{el}(\underline{x})[\phi(t, t_0) - \phi(t_r, t_0)] \quad \ldots\ldots (8)$$

where $w^{II}_{el}(\underline{x})$ is the elastic deflection at $\underline{x}$ based on elastic modulus $E(t_r)$ and is caused by unit uniform load on system II; $w^{II}_{el}(\underline{x})$ is calculated by a computer program based on a Fourier series solution according to the folded plate theory. The integral in Eq. 6 would normally be evaluated numerically by a summation.

To obtain the total deflections and stresses one must add to the values for system II the deflections and stresses on system I. Thus, the total deflections are $w(\underline{x}, t) = w^{I}(\underline{x}, t) + w^{II}(\underline{x}, t)$ where $w^{I}(\underline{x}, t) = w^{I}(\underline{x}, t_r) = w^{I}_{el}(\underline{x})\, E(t_0) J(t_r, t_0) = w^{I}_{el}(\underline{x})[1 + \phi(t_r, t_0)]$, in which $w^{I}_{el}(\underline{x})$ are the elastic deflections due to unit uniform load on system I, based on modulus $E(t_0)$. The deflection plots in our Figs. 5–9 give the values of $\Delta w(\underline{x}, t) = w(\underline{x}, t) - w(\underline{x}, t_r) = w^{I}(\underline{x}, t) + w^{II}(\underline{x}, t) - [w^{I}(\underline{x}, t_r) + w^{II}(\underline{x}, t_r)] = w^{I}(\underline{x}, t) - w^{I}(\underline{x}, t_r) + w^{II}(\underline{x}, t) = w^{II}(\underline{x}, t)$, as Eq. 3 indicates (note that $w^{II}(\underline{x}, t_r) = 0$ for $t \geq t_r$).

In all the calculations, the unit downward load is considered to be distributed uniformly over the total area of the top plate. The deflections are indicated in the figures for the intersection of web and top plate midplanes.

Appendix II.—References

1. American Concrete Institute Committee 209, Subcommittee II, "Prediction of Creep, Shrinkage, and Temperature Effects in Concrete Structures," *Designing for Creep and Shrinkage in Concrete*, American Concrete Institute Special Publication Number 76, Detroit, Mich., 1982, pp. 193–300.
2. Bažant, Z. P., "Prediction of Concrete Creep Effects Using Age-Adjusted Effective Modulus Method," *American Concrete Institute Journal*, Vol. 19, 1972, pp. 212–217.

3. Bažant, Z. P., "Comparison of Approximate Linear Methods for Concrete Creep," *Journal of the Structural Engineering Division*, ASCE, Vol. 99, No. 9, 1973, pp. 1851–1874.
4. Bažant, Z. P., "Theory of Creep and Shrinkage in Concrete Structure—A Précis of Recent Developments," *Mechanics Today*, Vol. 2, Pergamon Press, 1975, pp. 1–93.
5. Bažant, Z. P., and Chern, J. C., "Triple Power Law for Concrete Creep," *Journal of Engineering Mechanics*, ASCE, Vol. 111, No. 1, 1985, pp. 63–83.
6. Bažant, Z. P., and Křístek, V., "Effects of Shear Lag and Randomness of Material Properties on Deflections and Stresses in Prestressed Concrete Box Girder," *Preprints*, 4th RILEM International Symposium on Creep and Shrinkage of Concrete: Mathematical Modeling, Z. P. Bažant, Ed., held at Northwestern University, Evanston, Ill., Aug., 1986, pp. 675–684.
7. Bažant, Z. P., and Liu, K. L., "Random Creep and Shrinkage in Structures: Sampling," *Journal of Structural Engineering*, ASCE, Vol. 111, No. 5, 1985, pp. 1112–1134.
8. Bažant, Z. P., and Ong, J. S., "Creep in Continuous Beams Built Span-by-Span," *Journal of Structural Engineering*, ASCE, Vol. 109, No. 7, 1983, pp. 1648–1668.
9. Bažant, Z. P., and Panula, L., "Practical Prediction of Creep and Shrinkage of Concrete," *Materials and Structures*, Parts I and II, No. 69, 1978, 415–434; Parts III–IV, No. 70, 1978, pp. 415–434 and Parts V–VI, Vol. 72, 1979, pp. 169–183.
10. Bažant, Z. P., and Panula, L., "Creep and Shrinkage Characterization for Analyzing Prestressed Concrete Structures," *Prestressed Concrete Institute Journal*, Vol. 25, No. 3, 1980, pp. 86–122.
11. Bažant, Z. P., and Wittmann, F. H. (Eds.), *Creep and Shrinkage in Concrete Structures*, J. Wiley and Sons, New York, N.Y., 1982.
12. Blom, G., *Statistical Estimates and Transformed Data Variables*, J. Wiley, New York, N.Y., 1958.
13. DeFries-Skene, A., and Scordelis, A. C., "Direct Stiffness Solution for Folded Plates," *Journal of the Structural Division*, ASCE, Vol. 90, No. 4, 1964, pp. 15–47.
14. Kimball, B. F., "On the Choice of Plotting Positions on Probability Paper," *Journal of the American Statistical Association*, Vol. 55, No. 291, Sept., 1960, pp. 546–560.
15. Křístek, V., *Theory of Box Girders*, John Wiley and Sons, New York, N.Y., 1979.
16. Křístek, V., "Folded Plate Approach to Analysis of Shear Wall Systems and Frame Structures," *Proceedings*, Institute of Civil Engineers, Part 2, Vol. 67, Dec., 1979, pp. 1065–1075.
17. Křístek, V., "Shear Lag in Box Girders," *Plated Structures* (Chapter 6), R. Narayanan, Ed., Applied Science Publishers, 1983.
18. Křístek, V., and Evans, H. R., "A Hand Calculation of the Shear Lag Effect in Unstiffened Flanges and in Flanges with Closely Spaced Stiffeners," *Journal of Civil Engineering for Practicing and Design Engineers*, Vol. 4, No. 2, Jan., 1985.
19. Madsen, H. O., and Bažant, Z. P., "Uncertainty Analysis of Creep and Shrinkage Effects in Concrete Structures," *American Concrete Institute Journal*, Vol. 80, Mar.–Apr., 1983, pp. 116–127.
20. Martz, H. F., and Waller, R. A., *Bayesian Reliability Analysis*, J. Wiley and Sons, New York, N.Y., 1982.
21. RILEM Committee TC67, "Creep and Shrinkage of Concrete: Mathematical Modeling," *State-of-Art Report*, Preprints, 4th Intern. Symp. on Creep and Shrinkage of Concrete: Math. Modeling, held at Northwestern University, Evanston, Ill., Aug., 1986, Z. P. Bažant, Ed., pp. 39–455.
22. Scordelis, A. C., "Analytical Solutions for Box Girder Bridges," *Proc. of the Conference on Developments in Bridge Design and Construction*, Cardiff, U.K., 1971.